High-order thermal ghost imaging

Kam Wai Clifford Chan,* Malcolm N. O'Sullivan, and Robert W. Boyd

The Institute of Optics, University of Rochester, Rochester, New York 14627, USA
*Corresponding author: kwchan@optics.rochester.edu

We show theoretically that high-order thermal ghost imaging has considerably higher visibility and contrast-to-noise ratio than conventional thermal ghost imaging, which utilizes the lowest-order intensity cross correlation of the object and the reference signal. We also deduce the optimal power order of the correlation that gives the best contrast-to-noise ratio. © 2009 Optical Society of America

OCIS codes: 110.1650, 030.4280.

Ghost imaging is an indirect imaging method that acquires the image of an object through spatial-intensity-correlation measurements. In the imaging setup, two spatially correlated light fields are used: an object field that illuminates the object but is not spatially resolved by its detector and a reference field that does not interact with the object but is spatially resolved by its detector. Then, by measuring the intensity cross-correlation function of the object and reference fields, an image (the "ghost image") can be obtained. By separating the process of forming the image from that of interrogating the object, new possibilities for enhanced image formation and remote sensing are made possible.

The first ghost imaging experiment was realized by using the spatial entanglement of biphotons generated in spontaneous parametric downconversion [1]. It was subsequently demonstrated that nearly all features of ghost imaging can be replicated by using pseudothermal light [2–4]. This raises questions on whether the fundamental source of the correlation that gives rise to ghost imaging is of quantum or classical nature, despite the fact that thermal ghost imaging can be correctly analyzed without recourse to quantum theory [5–10].

In spite of the similarities between quantum and thermal ghost imaging, the main difference between the two concerns the visibilities $V = (I_{signal} - I_{bgd})/(I_{signal} + I_{bgd})$ of the ghost images formed in these two schemes, where I_{signal} and I_{bgd} are respectively the image and background signals. Quantum ghost imaging can in principle achieve 100% visibility. In contrast, the ghost image formed using thermal light always lies on a large background. More importantly, both the thermal ghost image and the background signal are very noisy [7,11]. Therefore, even though the background signal can be subtracted from the total signal, a large number of samplings of signals are required to obtain acceptable quality of the image in the thermal ghost imaging setup.

In a recent work, Cao *et al.* [12] showed that by using high-order correlation, the visibility of ghost diffraction can be improved. Nevertheless, a high visibility does not imply a good image; a high contrast-to-noise ratio (CNR) of the signal is also needed. In this Letter, we analyze high-order thermal ghost imaging using a classical argument and quantitatively show that both the visibility and the contrast of the

ghost image increase with the order of the correlation used. The CNR of a high-order ghost image is found to be maximum at some specific power order of the correlation, in contrast to the monotonically increasing improvement of the visibility when the orders of the correlation are increased [12]. We also obtain the scaling laws of the optimal CNR and the optimal order of the correlation on the ratio between the object size and the speckle size of the thermal light source. Our analytical results are compared with numerical simulations.

We consider the lensless ghost imaging configuration depicted in Fig. 1(a), which is assumed to be shot-noise limited. The ghost image is obtained by calculating the intensity–intensity correlation of the signals of the bucket detector and the reference detector (CCD camera),

$$G_{m,n}(x) = \frac{1}{N}\sum_{s=1}^{N} [I_o^{(s)}]^m [I^{(s)}(x)]^n, \qquad (1)$$

where N is the number of samplings,

$$I_o^{(s)} = \int dy\, O(y) I^{(s)}(y) \qquad (2)$$

is the sth signal of the bucket detector, and $I^{(s)}(x)$ is the sth signal of the reference detector. Here $O(y)$ is the object transmission function. For conventional thermal ghost imaging, $m = n = 1$. Note that the speckle pattern $I^{(s)}(x)$ on the CCD and the speckle pattern $I^{(s)}(y)$ on the object plane are identical, which
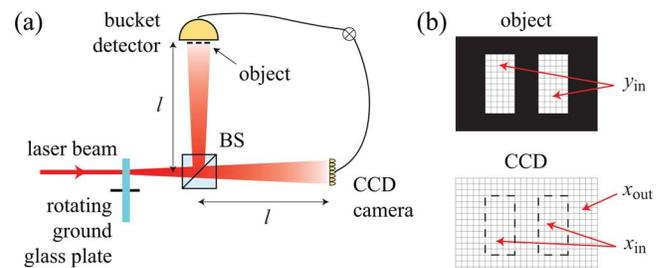
Fig. 1. (Color online) (a) Schematic representation of lensless thermal ghost imaging. (b) Simplified object model for analysis. The object plane (upper) and the reference detector plane (lower) are discretized by pixels of finite sizes. The light falling on a pixel is assumed to be statistically independent of that on other pixels.

© 2009 Optical Society of America

come from the propagated speckle patterns produced by the rotating ground-glass plate [4]. Therefore we can perform the analysis by considering directly the correlation of the light on the reference detector plane and the object plane, instead of that on the plane of the ground-glass plate. In writing Eq. (1), the light source is taken to be bright enough that the intensity fluctuations of the speckles dominate the signals of the detectors, so shot noise can be neglected. In addition, we assume in the following that the light source is ergodic and thermal and that its average intensity is uniform over the object surface with a negative exponential probability distribution $P(I,x)$ of mean $\langle I(x) \rangle \equiv \mu$ for all the positions x under the typical condition that the photodetector response time is short compared with the correlation time of the speckle field.

To simplify the analysis, we follow the method used in [11]. The object is taken to be a binary object, as depicted in Fig. 1(b). Moreover, we assume that the average size of the speckles of the pseudothermal light over the object surface is much smaller than the dimensions of the object and that it is about the same as the pixel size of the CCD camera. As a result, we can spatially discretize the intensity of light over the object surface. The sth signal of the bucket detector is then proportional to

$$I_o^{(s)} = \sum_{y_{\text{in}}}^{T} I^{(s)}(y_{\text{in}}), \qquad (3)$$

where $I^{(s)}(y_{\text{in}})$ is the intensity of light at pixel y_{in} inside the regions where light is transmitted and T is the number of illuminated pixels. In practice, T is proportional to the ratio of the transparent area of the object to the speckle size.

The mean value of the high-order cross-correlation of the object signal and reference signal is given by

$$\langle G_{m,n}(x_{\text{in}}) \rangle = \frac{(T+m+n-1)!n!}{(T+n-1)!}\mu^{m+n}, \qquad (4a)$$

$$\langle G_{m,n}(x_{\text{out}}) \rangle = \frac{(T+m-1)!n!}{(T-1)!}\mu^{m+n}, \qquad (4b)$$

where x_{in} and x_{out} are the pixels of the CCD camera that correspond to the pixels of the regions of the object where light is transmitted and blocked respectively [see Fig. 1(b)]. Note that, in calculating Eq. (4), we have used the relations $\langle [I^{(s)}(x)]^n \rangle = n!\mu^n$ and

$$\left\langle \left[\sum_{y_{\text{in}}}^{T} I^{(s)}(y_{\text{in}}) \right]^m \right\rangle = \frac{(T+m-1)!}{(T-1)!}\mu^m \qquad (5)$$

for thermal light. Equation (5) can be derived by noting that $I_o^{(s)}$ is a sum of $2T$ independent chi-squared random variables. On the other hand, the variance of the correlation is given by

$$[\Delta G_{m,n}(x)]^2 = \langle [G_{m,n}(x)]^2 \rangle - \langle G_{m,n}(x) \rangle^2$$
$$= [\langle G_{2m,2n}(x) \rangle - \langle G_{m,n}(x) \rangle^2]/N. \qquad (6)$$

Here we have taken the fact that the sth signal is uncorrelated with the s'th signal for $s \neq s'$. As a result, the visibility of the high-order ghost image is found to be

$$V_{m,n} = \frac{\langle G_{m,n}(x_{\text{in}}) \rangle - \langle G_{m,n}(x_{\text{out}}) \rangle}{\langle G_{m,n}(x_{\text{in}}) \rangle + \langle G_{m,n}(x_{\text{out}}) \rangle}$$
$$= 1 - 2\left[1 + \frac{(T+m+n-1)!(T-1)!}{(T+m-1)!(T+n-1)!} \right]^{-1} \qquad (7a)$$

$$\approx \tanh\left(\frac{mn}{2T} \right), \quad \text{for } T \gg m,n. \qquad (7b)$$

The quality of the ghost image is characterized by the CNR:

$$\text{CNR}_{m,n} = \frac{\langle G_{m,n}(x_{\text{in}}) \rangle - \langle G_{m,n}(x_{\text{out}}) \rangle}{\Delta G_{m,n}(x_{\text{in}}) + \Delta G_{m,n}(x_{\text{out}})}$$
$$= 2V_{m,n} \left/ \left(\frac{1+V_{m,n}}{\text{SNR}_{m,n}^{(\text{in})}} + \frac{1-V_{m,n}}{\text{SNR}_{m,n}^{(\text{out})}} \right) \right., \qquad (8)$$

where $\text{SNR}_{m,n}^{(i)} = G_{m,n}(x_i)/\Delta G_{m,n}(x_i)$ with $i=$ in and out are the signal-to-noise ratios inside and outside the transmitted regions. Note that the SNRs, and hence $\text{CNR}_{m,n}$, are proportional to $\sqrt{N}$.

The visibility and CNR are plotted in Fig. 2(a). Both quantities depend on the order indices m and n as well as the number of illuminated pixels T. The visibility is a monotonic increasing function of m and n, and it is largest when $m=n$. In contrast, the CNR attains maximum value (denoted by CNR_{opt}) at some particular values of m and n for a given T. As a comparison, results for numerical simulations using a one-dimensional double slit are shown in Fig. 2(b). The figures show that the analytical results agree quite well with the simulated results. The discrepancy appears when $n \gg m$. This is due to the large fluctuations of the reference signal $I(x)$, which are magnified tremendously when raised to the nth power with $n \gg 1$. On the contrary, the bucket signal I_o can be regarded as an average of $2T$ random signals [see Eq. (3)]. Thus the fluctuations of I_o are much smaller than that of $I(x)$. This also explains why the optimal CNR appears at small n. Figure 2(c) shows the reconstructed conventional and optimal ghost images.

Both the visibility and the CNR decrease when T increases. As Eq. (7b) shows, the visibility scales as $1/T$ when T is large. The corresponding scaling laws for the CNR are plotted in Fig. 3(a). The optimal CNR scales as $\sqrt{N/T}$, whereas the CNR for the conventional ghost imaging ($\text{CNR}_{1,1}$) scales as $\sqrt{N}/T$ for large T. Therefore there is obvious advantage of employing high-order correlation for thermal ghost imaging when small speckles are used to illuminate ob-
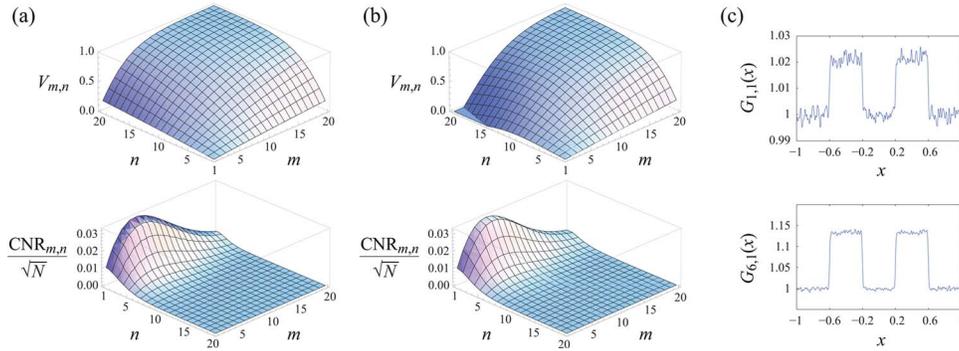
Fig. 2. (Color online) (a) Plots of the visibility $V_{m,n}$ and the contrast-to-noise ratio $\mathrm{CNR}_{m,n}/\sqrt{N}$ as functions of m and n using Eqs. (7a) and (8) with $T=45$. (b) Plots of $V_{m,n}$ and $\mathrm{CNR}_{m,n}/\sqrt{N}$ as functions of m and n for numerical simulations of a one-dimensional double slit using pseudothermal light. The field spatial correlation is given by $\langle E*(x)E(x')\rangle = \mu \exp(-(x-x')^2/(\Delta x)^2)$ with $\Delta x=0.01$, which gives a $\mathrm{CNR}_{\mathrm{opt}}$ that corresponds to $T\approx 45$. The speckle size $\Delta_{\mathrm{speckle}} \sim 2(\Delta x/\sqrt{2})$ and the number of speckles covering the slits $T_{\mathrm{speckle}}=0.8/\Delta_{\mathrm{speckle}}\approx 57$. The simulation grid size is 0.001. The number of samplings is taken to be $N=500{,}000$ to obtain good results for large n. (c) Reconstructed conventional ghost image $G_{1,1}(x)$ and optimal ghost image $G_{6,1}(x)$ with the background normalized to 1.

jects with large transparent regions. The bucket signal and the reference signal orders that give the optimal CNR are plotted in Fig. 3(b). For the range of T under consideration, the CNR is the largest when $n=1$ or 2, with the optimal m proportional to $\sqrt{T}$. Note that we have used a binary object to obtain the scaling laws in T. For a more general grayscale object, T will be given by an average object area divided by the speckle size [13], and the scaling laws in T should still be valid.
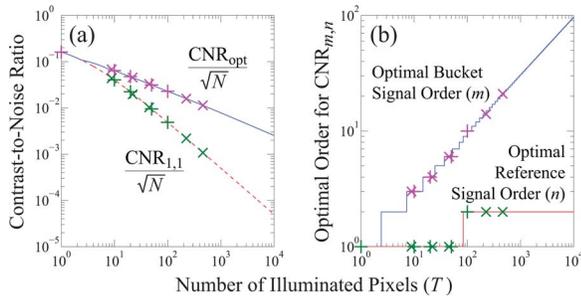
Fig. 3. (Color online) (a) Plot of the CNR as a function of T. The solid line shows the optimal CNR, whereas the dashed curve shows the CNR for conventional thermal ghost imaging. (b) Plots of the optimal bucket signal order m and reference signal order n for the CNR. The data points shown on the figures are from the numerical simulations using delta correlations (+) with $T=1$, 10, 20, 50, and 100, and Gaussian correlations $\langle E*(x)E(x')\rangle = \mu \exp(-(x-x')^2/(\Delta x)^2)$ (×) with $\Delta x=0.05$, 0.02, 0.01, 0.002, and 0.001. The effective Ts for the Gaussian cases are obtained by matching the calculated $\mathrm{CNR}_{\mathrm{opt}}$ with the theory and are found to be $T\approx 9$, 22, 45, 224, and 460. The number of speckles covering the slits $T_{\mathrm{speckle}}\approx 11$, 28, 57, 283, and 567 (see the caption of Fig. 2). The simulation grid size for the Gaussian correlation is 0.001, and that for the delta correlation is adjusted to give the desired values of T.

Finally, it is remarked that, by using a compressive sensing algorithm instead of the intensity correlation, both the visibility and the CNR of the reconstructed ghost image can also be greatly enhanced [14]. However, it is uncertain whether the compressive method is applicable to ghost diffraction.

References

1. T. B. Pittman, Y. H. Shih, D. V. Strekalov, and A. V. Sergienko, Phys. Rev. A **52**, R3429 (1995).
2. A. Gatti, E. Brambilla, M. Bache, and L. A. Lugiato, Phys. Rev. A **70**, 013802 (2004).
3. A. Valencia, G. Scarcelli, M. D'Angelo, and Y. H. Shih, Phys. Rev. Lett. **94**, 063601 (2005).
4. K. W. C. Chan, M. N. O'Sullivan, and R. W. Boyd, Phys. Rev. A **79**, 033808 (2009).
5. G. Scarcelli, V. Berardi, and Y. H. Shih, Phys. Rev. Lett. **96**, 063602 (2006).
6. A. Gatti, M. Bondani, L. A. Lugiato, M. G. A. Paris, and C. Fabre, Phys. Rev. Lett. **98**, 039301 (2007).
7. B. I. Erkmen and J. H. Shapiro, Phys. Rev. A **77**, 043809 (2008).
8. L.-G. Wang, S. Qamar, S.-Y. Zhu, and M. S. Zubairy, Phys. Rev. A **79**, 033835 (2009).
9. J. H. Shapiro, Phys. Rev. A **78**, 061802 (2008).
10. Y. Bromberg, O. Katz, and Y. Silberberg, Phys. Rev. A **79**, 053840 (2009).
11. L. Basano and P. Ottonello, Opt. Express **15**, 12386 (2007).
12. D.-Z. Cao, J. Xiong, S.-H. Zhang, L.-F. Lin, L. Gao, and K. Wang, Appl. Phys. Lett. **92**, 201102 (2008).
13. B. I. Erkmen and J. H. Shapiro, Phys. Rev. A **79**, 023833 (2009).
14. O. Katz, Y. Bromberg, and Y. Silberberg, Appl. Phys. Lett. **95**, 131110 (2009).